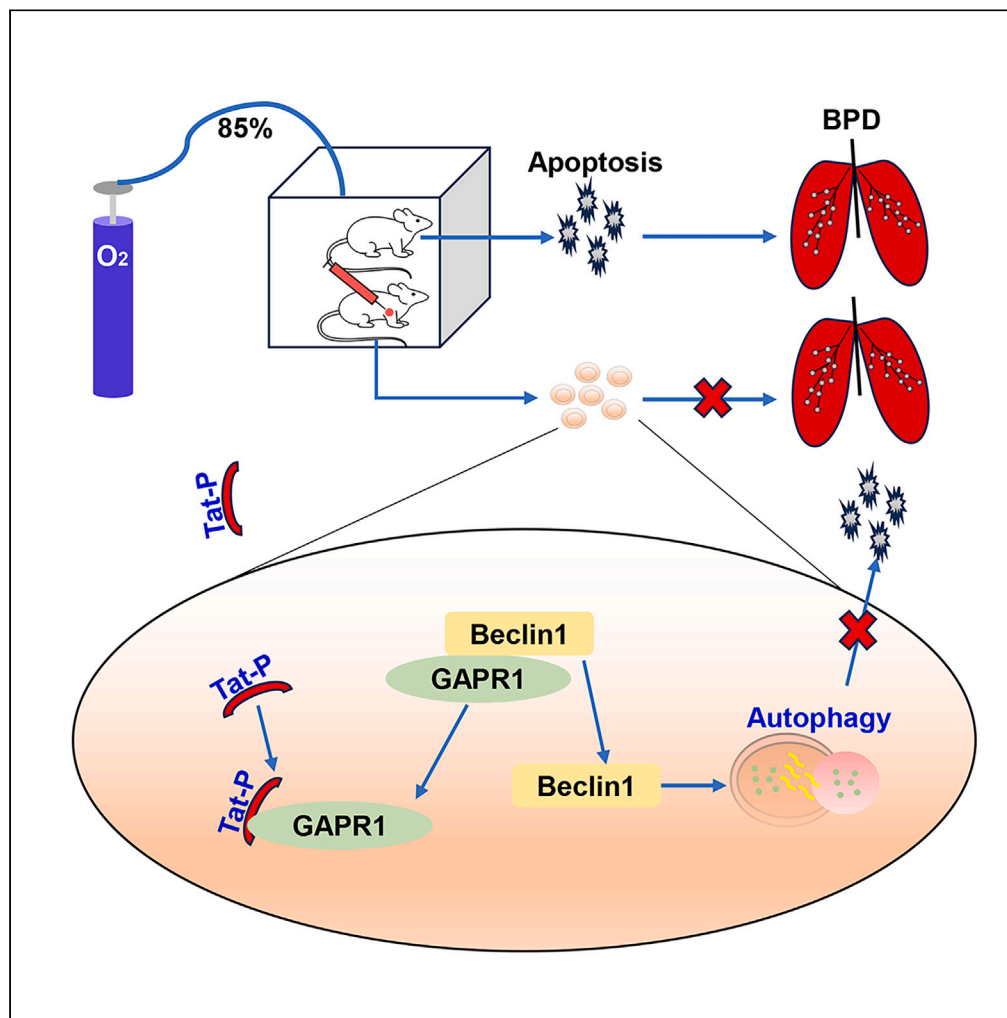


Article

# Tat-P combined with GAPR1 releases Beclin1 to promote autophagy and improve Bronchopulmonary dysplasia model



Yahui Zhou, Yuting Zhu, Weilai Jin, ..., Zhangbin Yu, Le Zang, Zhiwei Yu

yahuizhou@njmu.edu.cn (Y.Z.)  
yuzhangbin@126.com (Z.Y.)  
zhle@njmu.edu.cn (L.Z.)  
yu98204@aliyu.com (Z.Y.)

**Highlights**

Tat-P promoted autophagy and partially prevented apoptosis

Tat-P competitively binds to GAPR1 displacing the Beclin1 to prevent apoptosis

Tat-P promoted autophagy and reduced apoptosis ameliorated BPD-related phenotypes



## Article

## Tat-P combined with GAPR1 releases Beclin1 to promote autophagy and improve Bronchopulmonary dysplasia model

Yahui Zhou,<sup>1,5,6,\*</sup> Yuting Zhu,<sup>1,5</sup> Weilai Jin,<sup>1,5</sup> Ru Yan,<sup>1</sup> Yuanyuan Fang,<sup>1</sup> Fan Zhang,<sup>1</sup> Tonghui Tang,<sup>1</sup> Si Chen,<sup>1</sup> Jing Chen,<sup>1</sup> Fan Zhang,<sup>3</sup> Zhangbin Yu,<sup>2,4,\*</sup> Le Zang,<sup>1,\*</sup> and Zhiwei Yu<sup>1,\*</sup>

## SUMMARY

**Long-term exposure to hyperoxia can leading to the bronchopulmonary dysplasia (BPD). The progression of BPD is primarily driven by the apoptosis of alveolar epithelial cells, and the regulation of autophagy has an impact on apoptosis. This study aims to investigate the therapeutic potential and underlying mechanism of an autophagy-promoting peptide (Tat-P) in ameliorating BPD. *In vitro* experiments demonstrated that Tat-P promoted autophagy and partially prevented apoptosis caused by exposure to hyperoxia. Further investigation into the mechanism revealed that Tat-P competitively binds to GAPR1, displacing the Beclin1 protein and thereby inhibiting the apoptosis. *In vivo* experiments conducted on Sprague-Dawley pups exposed to high oxygen levels demonstrated that Tat-P promoted autophagy and reduced apoptosis in lung tissues and ameliorated BPD-related phenotypes. Our findings elucidate the underlying mechanisms and effects of Tat-P in enhancing autophagy and preventing apoptosis. This study presents an approach for the prevention and treatment of BPD.**

## INTRODUCTION

Bronchopulmonary dysplasia (BPD) is a common complication observed in preterm births, particularly in extremely preterm infants, and it has significant long term prognostic implications.<sup>1</sup> BPD is believed to arise from complex interactions between prenatal and postnatal factors, including essential interventions such as oxygen therapy and mechanical ventilation, which are critical for the survival of premature infants.<sup>2,3</sup> Nevertheless, the precise molecular mechanisms underlying the development of BPD remain incompletely understood.

Previous investigations have demonstrated the crucial role of autophagy in normal lung development and morphogenesis.<sup>4,5</sup> Conversely, autophagy is substantially impaired in the lung tissues of BPD animal models.<sup>6</sup> However, the introduction of an autophagy activator has been shown to effectively ameliorate apoptosis and restored impaired alveolar development in hyperoxia-induced BPD models using Sprague–Dawley (SD) pups.<sup>7</sup> Thus, the activation of autophagy represents a promising avenue for the prevention and treatment of BPD.

Beclin1, a mammalian counterpart of yeast Atg6, plays a pivotal role in autophagy regulation.<sup>8,9</sup> Manipulation of Beclin1 to promote autophagy presents a potential strategy for preventing and treating BPD. The regeneration of alveolar epithelial cells is crucial for the structural and functional repair of the alveoli,<sup>10,11</sup> and the apoptosis of alveolar epithelial cells is a critical factor contributing to the development of BPD.<sup>12</sup> Beclin1 exhibits anti-apoptotic effects in various contexts, including tumor necrosis factor-related apoptosis-inducing ligand, chemotherapy, radiation therapy, immunotherapy, nutrient deprivation, and angiogenesis inhibition.<sup>9</sup> Therefore, investigating the interplay between Beclin1-mediated autophagy regulation and apoptosis may yield insights into the prevention and treatment of BPD.

Tat-P, an amino acids sequence within the Beclin1 domain,<sup>13</sup> competes with the Beclin1 protein for binding to GAPR1 (an autophagy inhibitory protein<sup>14</sup>). Our study revealed that Tat-P binds to GAPR1, releasing Beclin1 and thereby promoting autophagy to inhibit apoptosis and repair alveolar epithelial cell damage induced by hyperoxia. Additionally, Tat-P improved pathological features associated with BPD, such as

<sup>1</sup>Department of Neonatology, Wuxi Children's Hospital affiliated to Jiangnan University, Wuxi, China

<sup>2</sup>Department of Neonatology, Shenzhen People's Hospital, The Second Clinical Medical College, Jinan University, Shenzhen, Guangdong, China

<sup>3</sup>Department of Pediatrics, Affiliated Maternity and Child Health Care Hospital of Nantong University, Nantong, China

<sup>4</sup>The First Affiliated Hospital, Southern University of Science and Technology, Shenzhen, Guangdong, China

<sup>5</sup>These three authors contributed equally

<sup>6</sup>Lead contact

\*Correspondence: yahuizhou@njmu.edu.cn (Y.Z.),

yuzhangbin@126.com (Z.Y.), zhle@njmu.edu.cn (L.Z.), yu98204@aliyu.com (Z.Y.)

<https://doi.org/10.1016/j.isci.2023.107509>



lung structure collapse, alveolar fusion, and widened alveolar septa resulting from high oxygen exposure. Consequently, the clinical application of this peptide may offer an approach to the prevention and treatment of BPD.

## RESULTS

### Basic characteristics of Tat-P

Beclin1, a pro-autophagy protein, contains a functional domain whose amino acid sequence 267–284 has been validated to enhance autophagy. To target this sequence, we synthesized a cell permeable peptide using *in vitro* synthesis and named it Tat-P. Additionally, we synthesized a scrambled peptide with the same amino acids but in a different sequence, named Tat-Scr, using the same method (Figure 1A). Bioinformatics analysis revealed that Tat-P had an estimated half-life of approximately 7.5 h and displayed strong lipophilic activity (Figure 1B). Furthermore, fluorescence microscopy demonstrated that GFP-labeled Tat-P effectively entered alveolar epithelial cells within 3 h (Figure 1C). We also examined the entry of GFP alone, GFP + Tat-P, and GFP + Tat-Scr. Fluorescence microscopy confirmed that both GFP-Tat-P and GFP-Tat-Scr could enter alveolar epithelial cells within 3 h (Figure 1D). However, only GFP + Tat-P promoted autophagy (Figure S1C). Moreover, *in vivo* imaging revealed that GFP-Tat-P successfully reached various organs, including the liver, spleen, and lungs, in pups within 6 h of intraperitoneal injection (Figure 1E). This observation lays the groundwork for investigating its biological role in specific organs and cells.

### Tat-P repairs hyperoxia-induced cell damage *in vitro*

We observed that Tat-P restored autophagy inhibition caused by hyperoxia in both cell and animal models of BPD (Figures S1A and S1B). This finding prompted us to explore whether Tat-P could serve as a potential therapeutic agent for BPD. In our study, we assessed the impact of Tat-P intervention on oxidative stress in alveolar epithelial cells. We found that hyperoxia exposure increased ROS levels in these cells, while treatment with Tat-P at different concentrations (1, 2.5 and 5  $\mu$ M) reduced ROS levels in a concentration-dependent manner (Figure 2A). Importantly, Tat-P exhibited no toxicity toward alveolar epithelial cells under normal oxygen conditions, and it improved the decreased cell viability induced by hyperoxia exposure (Figures 2B and 2C), as demonstrated by the CCK8 assay. Flow cytometry analysis revealed that Tat-P intervention also concentration-dependently attenuated the elevated apoptosis resulting from high oxygen exposure (Figure 2D). In contrast, Tat-Scr (Tat-scrambled) did not rescue the decreased cell viability or the increased cell apoptosis induced by hyperoxia (Figures S2A–S2C). Additionally, we evaluated the expression of the type II alveolar epithelial cell surface marker SPC and found that Tat-P intervention restored the downregulation of SPC protein expression caused by hyperoxia (Figure 2E). These results collectively indicate that Tat-P repairs hyperoxia-induced damage to alveolar epithelial cells at the cellular level.

### Tat-P improves alveolar epithelial cell injury by inhibiting apoptosis

Our findings demonstrate that Tat-P intervention effectively improves the apoptotic phenotype induced by hyperoxia, prompting us to investigate how Tat-P inhibits apoptosis in alveolar epithelial cells. Mitochondrial membrane potential disruption is often associated with apoptosis and is considered an early event in the apoptotic process. To assess mitochondrial membrane potential in cells, we employed the JC-1 kit. In cells with normal membrane potential, JC-1 enters the mitochondria forms a red fluorescent polymer due to increased concentration resulting from mitochondrial membrane polarity. In apoptotic cells with depolarized membrane potential, JC-1 is released from the mitochondria, leading to a decrease in concentration and a transition to a monomeric form that emits green fluorescence. Notably, cells in the hyperoxia group exhibited prominent green fluorescence, whereas those in the Tat-P + hyperoxia group displayed enhanced red fluorescence, particularly with increasing Tat-P concentration (Figure 3A). Subsequently, we assessed the expression of the anti-apoptotic protein Bcl-2 and the pro-apoptotic protein Bax. Our results revealed that Bcl-2 levels significantly decreased and Bax levels significantly increased in the hyperoxia group, while the Tat-P + hyperoxia group exhibited significantly elevated Bcl-2 expression and reduced Bax expression compared to the hyperoxia group (Figure 3B). These findings further corroborate the ability of Tat-P to attenuate apoptosis in hyperoxia-induced alveolar epithelial cells. Taken together, our results suggest that Tat-P may promote autophagy and inhibit apoptosis as a potential therapeutic strategy for BPD.

### Inhibition of autophagy prevents Tat-P from repairing alveolar epithelial cell damage

To further elucidate the role of Tat-P in promoting autophagy and repairing alveolar epithelial cell damage, we conducted additional experiments using autophagy inhibitors. Based on the results of cell viability and

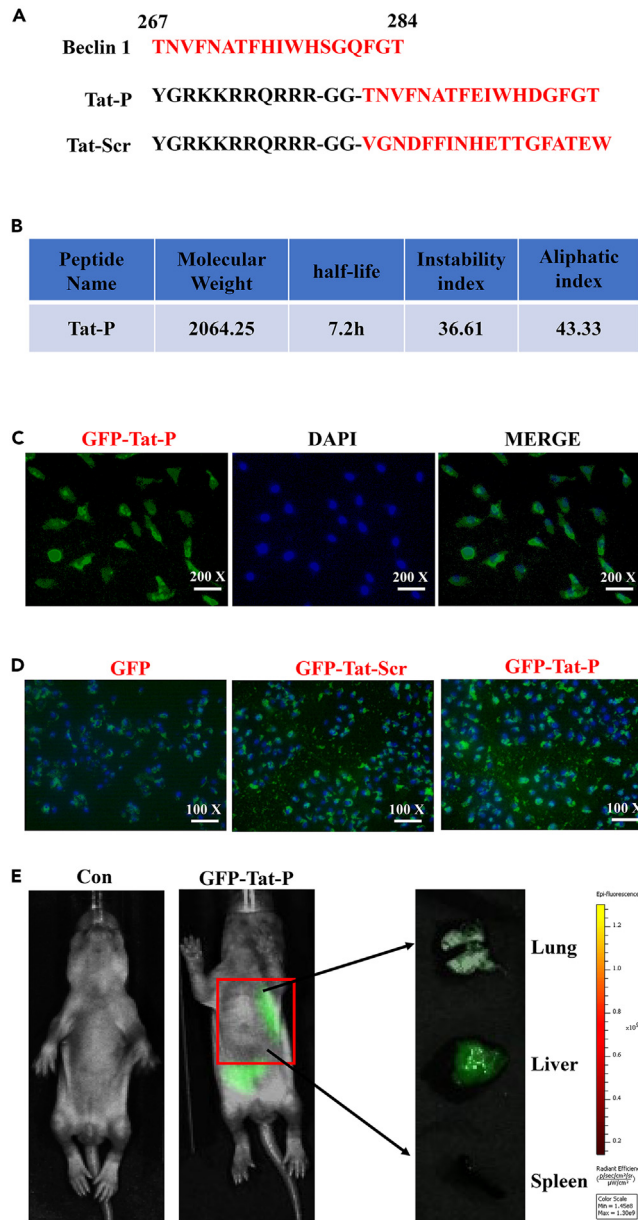


**Figure 1. Basic characteristics of Tat-P**

(A) Amino acid sequence of Tat-P in Beclin1 protein, and chemical synthesis of Tat-P and Tat-Scr sequences.

(B) Analysis of basic characteristics of Tat-P.

(C) Fluorescence microscope was used to evaluate the cell entry ability of GFP-Tat-P.

(D) fluorescence microscope was used to evaluate the cell entry ability of GFP, GFP-Tat-Scr, GFP-Tat-P.

(E) *In vivo* imaging was used to evaluate the distribution of Tat-P in tissues after intraperitoneal injection. Tat-Scr: Tat-scrambled.

apoptosis, we determined the optimal concentration of Tat-P to be 5  $\mu$ M. Western blotting analysis revealed a significant increase in the ratio of LC3II/LC3I and an elevation in P62 protein levels in the hyperoxia group compared to the control group. Importantly, the Tat-P + hyperoxia group exhibited a more pronounced increase in the LC3II/LC3I ratio and a significant reduction in P62 protein levels compared to the hyperoxia group. These findings indicate that hyperoxia inhibits autophagy in alveolar epithelial cells, while Tat-P administration restores hyperoxia-induced autophagy inhibition. Furthermore, the CQ group showed a significant increase in the LC3II/LC3I ratio and P62 protein levels compared to the control group, indicating

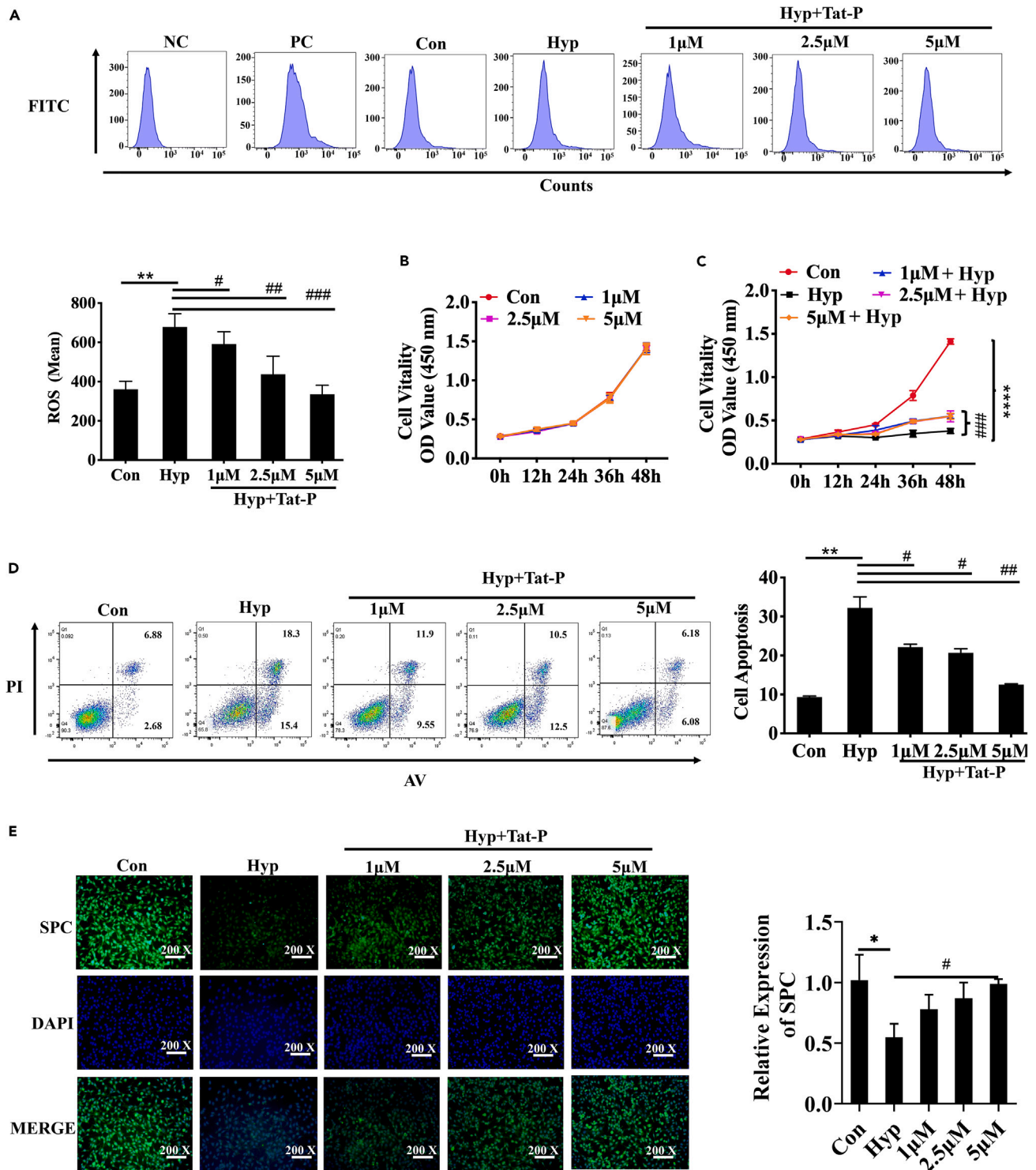


**Figure 2. Tat-P repairs hyperoxia-induced cell damage *in vitro***

(A) ROS expression in MLE-12 cells of NC, PC, Con, Hyp, Hyp+Tat-P (1, 2.5 and 5μM) group, N = 3. Unpaired t-test.

(B) CCK8 was used to detect cell viability in MLE-12 cells of Con, Tat-P (1, 2.5 and 5μM) group, N = 3.

(C) CCK8 was used to detect cell viability in MLE-12 cells of Con, Hyp, Hyp+Tat-P (1, 2.5 and 5μM) group, N = 3.

(D) Flow cytometry was used to detect apoptosis in MLE-12 cells of Con, Hyp, Hyp+Tat-P (1, 2.5 and 5μM) group, N = 3.

**Figure 2. Continued**

(E) Immunofluorescence was used to detect SPC protein expression in MLE-12 cell line of Con, Hyp, Hyp+Tat-P (1, 2.5 and 5 $\mu$ M) group, N = 3, bar = 200x. Unpaired t-test, \*/#/p < 0.05, \*\*/##/p < 0.01, \*\*\*/###/p < 0.001, \*\*\*\*/####/p < 0.0001. NC: Negative control, PC: Positive control, Con: control, Hyp: Hyperoxia. \* VS. Con, # VS. Hyp.

autophagy inhibition by CQ. Notably, in the CQ + Tat-P group, the LC3II/LC3I ratio was higher than that in the CQ group, and the P62 protein levels were lower than those in the CQ group. These results suggest that CQ and hyperoxia further suppress autophagy, but Tat-P intervention partially restores autophagy in the presence of hyperoxia and CQ (Figure 4A). CCK8 analysis demonstrated that CQ inhibited cell viability under normal oxygen conditions, Tat-P had no toxic effect on cell viability and partially restored the inhibitory effect of CQ on cell viability (Figure 4B). Moreover, the CQ + hyperoxia group exhibited reduced cell viability compared to the hyperoxia group, whereas the Tat-P + hyperoxia + CQ group restored the decreased cell viability caused by the hyperoxia + CQ group (Figure 4C). Flow cytometry analysis indicated that the CQ + hyperoxia group displayed increased apoptosis compared to the hyperoxia group, whereas the Tat-P + CQ + hyperoxia group attenuated the increased apoptosis observed in the hyperoxia + CQ group (Figure 4D). Additionally, the CQ + hyperoxia group showed inhibited SPC expression, while the Tat-P + CQ + hyperoxia group rescued the decreased SPC levels induced by the hyperoxia + CQ group (Figure 4E). We further confirmed our findings using another autophagy inhibitor, 3MA. The 3MA + hyperoxia group exhibited further inhibition of autophagy compared to the hyperoxia group, and Tat-P partially restored autophagy in the presence of hyperoxia and 3MA (Figure S3A). Moreover, Tat-P rescued the decreased cell viability induced by 3MA (Figure S3B), and ameliorated the reduced cell viability and inhibited cell apoptosis caused by 3MA + hyperoxia (Figures S3C–S3E). These results collectively demonstrate that hyperoxia suppresses autophagy, whereas Tat-P promotes autophagy and ameliorates hyperoxia-induced cell damage.

**Inhibiting autophagy prevents Tat-P from repairing alveolar epithelial cell apoptosis**

We further investigated the effect of Tat-P on cell apoptosis by enhancing autophagy. Using the JC-1 kit, we observed that the CQ + hyperoxia group displayed higher levels of green fluorescence compared to the hyperoxia group, while the Tat-P + CQ + hyperoxia group exhibited reduced green fluorescence compared to the CQ + hyperoxia group (Figure 5A). Moreover, western blotting analysis revealed a significant decrease in Bcl-2 protein levels and a significant increase in Bax protein levels in the CQ + hyperoxia group compared to the hyperoxia group. However, the Tat-P + CQ + hyperoxia group, showed a significant increase in Bcl-2 protein levels and a significant decrease in Bax protein levels compared to the CQ + hyperoxia group (Figure 5B). These findings collectively indicate that Tat-P promotes autophagy to suppress hyperoxia-induced cell apoptosis.

**Tat-p promotes autophagy by binding to GAPR1 to release Beclin1**

We aimed to investigate the mechanism by which Tat-P promotes autophagy. Previous studies have shown that the interaction between Beclin1 and Bcl-2 proteins plays a role in inhibiting autophagy and promoting apoptosis. We hypothesized that Tat-P could bind to Bcl-2 protein and release Beclin1, thereby promoting autophagy and inhibiting apoptosis. However, our co-immunoprecipitation (CO-IP) assay results demonstrated that Tat-P does not bind to Bcl-2 protein (Figure S4A). We also examined the expression of Beclin1 protein in alveolar cells and lung tissues but did not observe any significant differences (Figures S4B and S4C). Interestingly, other studies have suggested that Tat-P can bind to the GAPR1 protein and release Beclin1 leading to autophagy promotion. To further explore this possibility, we repeated the CO-IP assay and confirmed that Tat-P indeed binds to GAPR1 protein (Figure 6A). Moreover, the binding between GAPR1 and Beclin1 was significantly reduced in the presence of Tat-P (Figure 6B). We also investigated the expression of GAPR1 under hyperoxic conditions and observed an increase in its expression (Figure 6C). Based on these findings, we propose that Tat-P may competitively bind to GAPR1, resulting in the release of Beclin1 and subsequently promoting autophagy while inhibiting apoptosis.

**Tat-p repairs the inhibition of cell autophagy induced by GAPR1 overexpression**

In order to provide additional evidence for the competitive binding of Tat-P to GAPR1 protein and its role in promoting autophagy in alveolar epithelial cells, we conducted experiments to overexpress GAPR1 using lentivirus. Fluorescence microscopy results demonstrated successful cell entry of the GAPR1 virus at titers of 1:20 and 1:40, 72 h post-transfection (Figure 7A). Therefore, we selected a titer of 1:20 for subsequent experiments. RT-qPCR and Western blotting analyses confirmed efficient transfection at this titer (Figures 7B and 7C). Furthermore, our CO-IP results revealed a significant increase in the binding of Beclin1 protein to

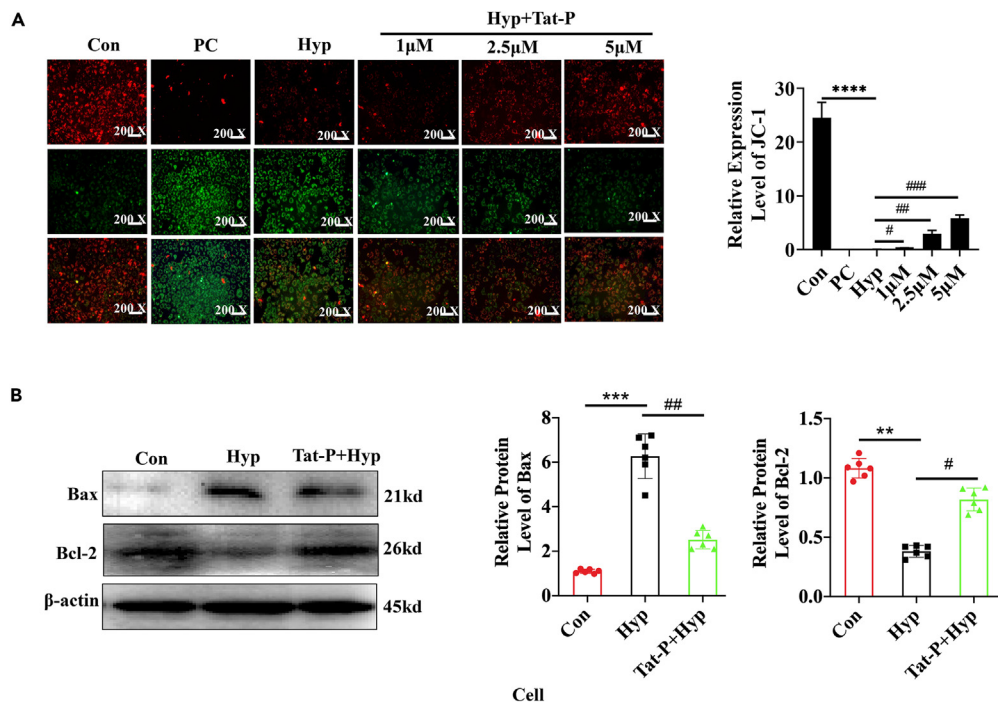


**Figure 3. Tat-P improved alveolar epithelial cell injury by inhibiting apoptosis**

(A) JC-1 kit was used to detect mitochondrial membrane potential in MLE-12 cells of Con, Hyp and Tat-P+Hyp group. Red fluorescence indicates living cells that maintain mitochondrial membrane potential, while green fluorescence indicates cells that have undergone apoptosis or necrosis, N = 3, bar = 200x.

(B) Western blot revealed the protein expression of Bax and Bcl-2 in MLE-12 cells of Con, Hyp and Tat-P+Hyp group, N = 6. Unpaired t-test, \*/#/p < 0.05, \*\*/##/p < 0.01, \*\*\*/###/p < 0.001, \*\*\*\*/####/p < 0.0001. Con: control, Hyp: Hyperoxia \* VS. Con, # VS. Hyp.

GAPR1 protein following GAPR1 transfection (Figure 7D). Western blotting analysis also showed a significant increase in p62 protein expression in the GAPR1 overexpression group, which was inhibited by Tat-P (Figure 7E). Moreover, in the GAPR1 + hyperoxia group, there was a further elevation in p62 expression, while Tat-P partially attenuated this increase (Figure 7E). Collectively, these findings provide further support for the notion that Tat-P promotes autophagy by competitively binding to GAPR1 and releasing Beclin1.

### Tat-P repairs alveolar epithelial cell damage caused by GAPR1 overexpression

In order to further investigate the binding of Tat-P to GAPR1 protein and its role in promoting autophagy and mitigating alveolar epithelial cell injury, we conducted additional experiments. Cell viability was assessed using a CCK8 kit, and the results demonstrated that overexpression of GAPR1 led to decreased cell viability. However, Tat-P treatment restored the reduced cell viability induced by GAPR1 overexpression. Similarly, in the GAPR1+ hyperoxia group, there was a further decline in cell viability, which was partially recovered by Tat-P (Figure 8A). Furthermore, RT-qPCR and immunofluorescence analyses revealed that Tat-P analyses revealed the decreased expression of SPC caused by GAPR1 overexpression. Conversely, in the GAPR1+ hyperoxia group, SPC expression was further inhibited, but Tat-P partially restored its expression (Figures 8B and 8C). Specific primer sequences are shown in Table 1. JC-1 kit and western blotting results demonstrated that Tat-P attenuated apoptosis induced by GAPR1 overexpression, and in the GAPR1 + hyperoxia group, apoptosis was further promoted. Tat-P still partially restored the apoptotic levels (Figures 8D and 8E). These rescue experiments provided additional evidence supporting the notion that Tat-P binds to GAPR1, leading to the release of Beclin1, thereby promoting autophagy and inhibiting apoptosis to repair alveolar epithelial cell damage. This novel approach may hold promise for the prevention and treatment of BPD.

### Tat-P ameliorates the hyperoxia-induced BPD model *in vivo*

To further investigate the potential of Tat-P in improving BPD, we conducted an animal study using an 85% hyperoxia exposure induced BPD model. The experimental groups included an air control group, a

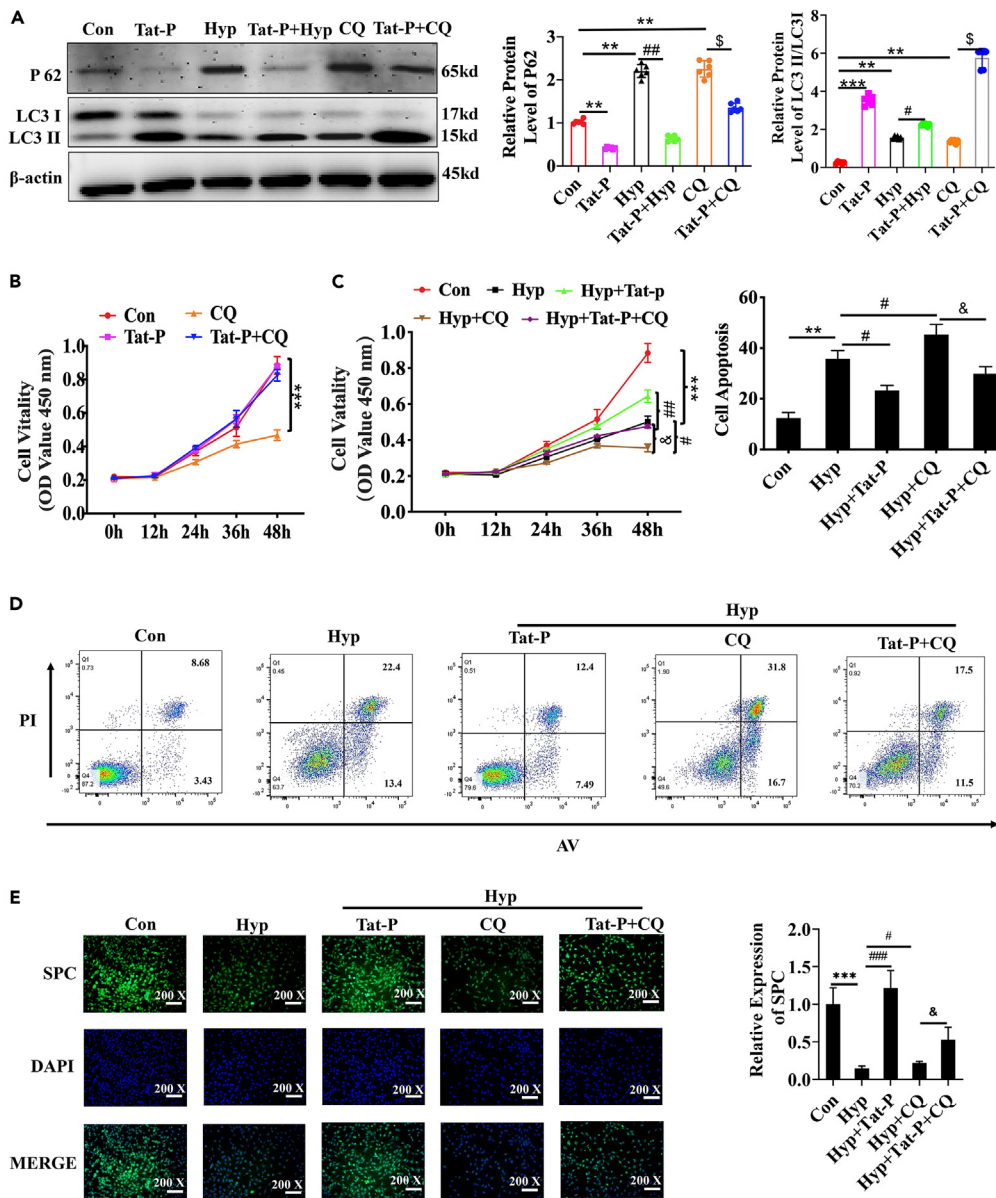


**Figure 4. Inhibition of autophagy prevents Tat-P from repairing alveolar epithelial cell damage**

(A) Western blot revealed the protein expression of P62 and LC3II/LC3I in MLE-12 cells of Con, Tat-P, Hyp, Tat-P + Hyp, CQ, Tat-P + CQ group, N = 6.

(B) CCK8 was used to detect cell-viability in MLE-12 cells of Con, Tat-P, CQ, Tat-p + CQ group, N = 3.

(C) CCK8 was used to detect cell viability in MLE-12 cells of Con, Hyp, Hyp + Tat-P, Hyp + CQ, Hyp + Tat-p + CQ group, N = 3.

(D) flow cytometry was used to detect apoptosis in MLE-12 cells of Con, Hyp, Hyp + Tat-P, Hyp + CQ, Hyp + Tat-p + CQ group, N = 3.

(E) Immunofluorescence was used to detect SPC protein expression level in MLE-12 cell line of Con, Hyp, Hyp + Tat-P, Hyp + CQ, Hyp + Tat-p + CQ group, N = 6, bar = 200x. Unpaired t-test, \*/#/\$/& p < 0.05, \*\*/##/\$\$/&& p < 0.01, \*\*\*/###/\$\$\$/&&& p < 0.001, \*\*\*\*/####/\$\$\$\$/&&&& p < 0.0001. Con: control, Hyp: Hyperoxia \* VS. Con, # VS. Hyp, \$ VS. CQ, & VS. Hyp + CQ.

hyperoxia model group, and a hyperoxia model group with Tat-P intervention. Throughout the modeling process, we monitored the daily changes in body weight of the pups. We observed a significant decrease in body weight of the pups in the hyperoxia model group compared to the air control group. However, in the hyperoxia model group with Tat-P intervention, there was a significant increase in body weight (Figure 9A).

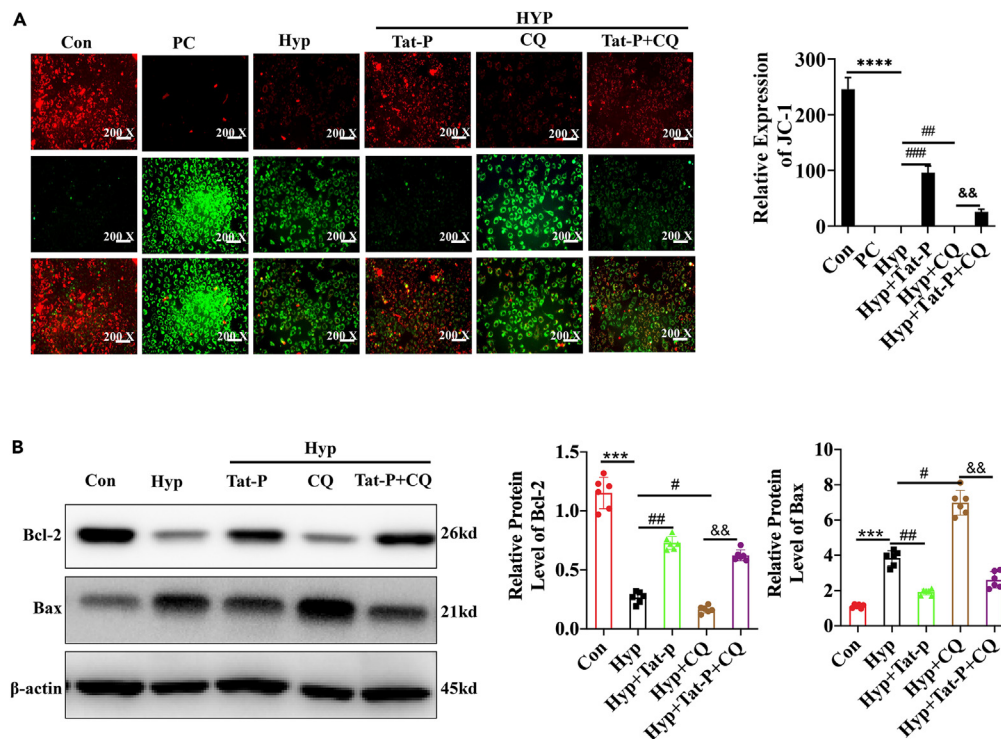


**Figure 5. Inhibiting autophagy prevents Tat-P from repairing alveolar epithelial cell apoptosis**

(A) JC-1 kit was used to detect mitochondrial membrane potential in MLE-12 cell line of Con, PC, Hyp, Tat-P + Hyp, CQ + Hyp and Tat-P + CQ + Hyp group, N = 3. Red fluorescence indicates living cells that maintain mitochondrial membrane potential, while green fluorescence indicates cells that have undergone apoptosis or necrosis, bar = 200x.

(B) Western blot revealed the protein expression of Bax and Bcl-2 in MLE-12 cells of Con, Hyp, Tat-P + Hyp, CQ + Hyp and Tat-P + CQ + Hyp group, N = 6. Unpaired t-test, \*#//& p < 0.05, \*\*##/∞∞ p < 0.01, \*\*\*/###/∞∞∞ p < 0.001, \*\*\*\*/####/∞∞∞∞ p < 0.0001. Con: control, Hyp: Hyperoxia \* VS. Con, # VS. Hyp, & VS. Hyp + CQ.

On the 7th day of modeling, the pups were sacrificed, and lung tissues were collected. Macroscopic examination of the lung tissues revealed significant collapse and shrinkage in the hyperoxia model group compared to the air control group. Remarkably, the lung tissues in the hyperoxia model group with Tat-P intervention showed significant recovery (Figure 9B). Histopathological analysis using H&E staining demonstrated notable improvement in the lung structure of the hyperoxia + Tat-P group, characterized by an increase in the number of alveoli and a decrease in alveolar septal thickness (Figure 9C). Immunohistochemistry results indicated a significant increase in the proliferation index (Ki67) and a significant decrease in the apoptosis index (TUNEL) in the hyperoxia + Tat-P group (Figures 9D and 9E). Furthermore, Tat-P inhibited the expression of Bax and promoted the expression of Bcl-2 in the animal models (Figure 9F). To further elucidate the reparative effect of Tat-P on alveolar epithelial cells *in vivo*, we assessed the expression of SPC using RT-qPCR and western blotting. The hyperoxia + Tat-P intervention group showed significant upregulation of SPC expression compared to the hyperoxia model group (Figures 9G and 9H). Specific primer sequences are shown in Table 1. In contrast, intervention with Tat-scrambled did not improve the observed weight loss, lung structure collapse, reduction of alveoli, or widening of alveolar septa induced by hyperoxia exposure (Figures S2D–S2F). These findings suggest that Tat-P can effectively repair alveolar epithelial cell damage and improve both the phenotypic and molecular characteristics of BPD animal models.

## DISCUSSION

Hyperoxia-induced BPD leads to impaired autophagy activity in the lungs of neonatal rats and baboons.<sup>15</sup> Previous studies have demonstrated that autophagy activators can reduce abnormal alveolar degeneration in BPD rats.<sup>7,16</sup> Tat-P, a peptide derived from the functional domain of the beclin1 protein, has been shown to promote autophagy.<sup>13</sup> During embryonic lung development, autophagy plays a crucial role in the

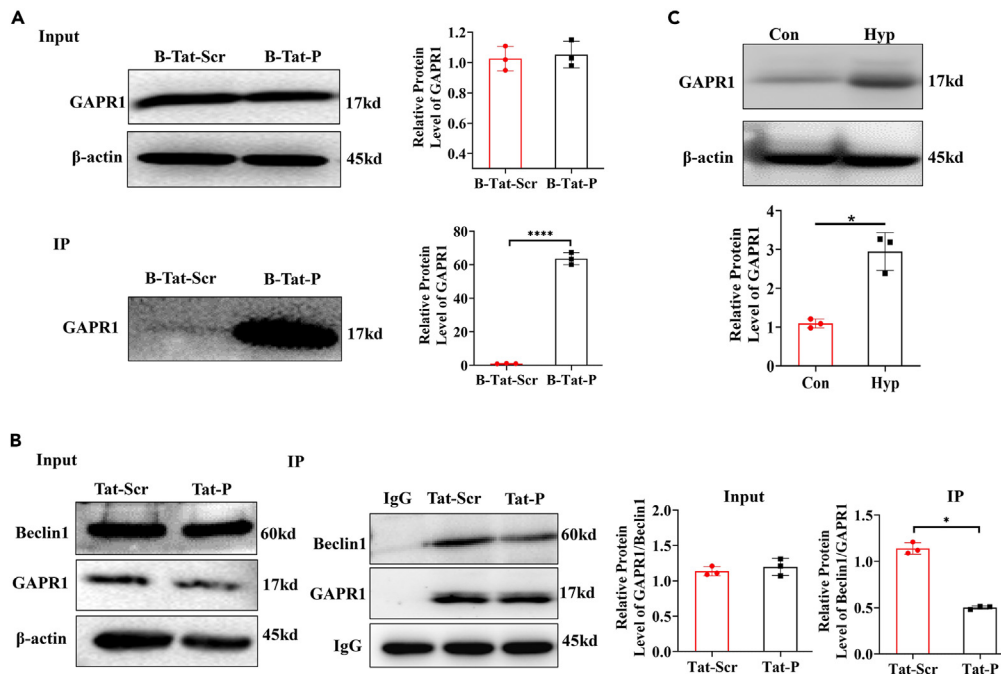


**Figure 6. Tat-P promotes autophagy by binding to GAPR1 to release Beclin1**

(A) CO-IP revealed the combination of GAPR1 and Tat-P in MLE-12 cells of B-Tat-S and B-Tat-P group, N = 3.

(B) CO-IP revealed the combination of GAPR1 and Beclin1 in MLE-12 cells of Tat-S and Tat-P group, N = 3.

(C) Western blot revealed the GAPR1 expression in Con and Hyp group, N = 3. Unpaired t-test, \*p < 0.05, \*\*p < 0.01, \*\*\*p < 0.001, \*\*\*\*p < 0.0001. Con: control, Hyp: Hyperoxia, B = Biotin. \* VS. Con or B-Tat-S.

maturation of lung epithelial cells.<sup>5,17</sup> Repairing alveolar epithelial cells is vital for treating lung injury associated with BPD and has been extensively studied to elucidate the molecular mechanisms underlying BPD.<sup>10,18,19</sup> In our study, we observed that Tat-P readily entered alveolar epithelial cells promoting autophagy and reversing the autophagy inhibition caused by hyperoxia. This suggests that Tat-P induces autophagy in alveolar epithelial cells and promotes cellular repair, which has implications for preventing and treating BPD.

BPD can arise from mechanical damage to lung tissue and alveolar epithelial cells resulting from excessive or prolonged oxygen exposure,<sup>20,21</sup> This damage is characterized by increased oxidative stress,<sup>22</sup> reduced cell viability,<sup>23</sup> increased apoptosis<sup>24,25</sup> and loss of alveolar epithelial cell surface markers.<sup>26</sup> Our findings align with the characteristic damage observed in BPD, as Tat-P effectively repaired the elevated ROS levels, restored cell viability, reduced apoptosis, and restored expression of the alveolar epithelial cell surface marker SPC in the presence of hyperoxia.

The decline in mitochondrial membrane potential is a critical early indicator of apoptosis.<sup>27</sup> When the mitochondrial membrane potential collapses, apoptosis becomes inevitable. Our findings demonstrated that Tat-P can restore the reduction in mitochondrial membrane potential caused by hyperoxia. The mitochondrial pathway is recognized as the classical pathway among the complex mechanisms of apoptosis.<sup>28</sup> The pro-apoptotic protein Bax can be insert into the outer membrane of mitochondria, initiating a cascade that leads to the release of apoptotic factors, the decline in mitochondrial membrane potential, and the promotion of cell apoptosis.<sup>29</sup> Bcl-2, on the other hand, can inhibit apoptosis by interacting with Bax.<sup>30</sup> In our study, we observed that Tat-P restored the mitochondrial membrane potential in hyperoxia-induced alveolar epithelial cells, suppressed Bax expression, and enhanced Bcl-2 expression. Given that BPD develops through the apoptosis of alveolar epithelial cells due to oxidative stress injury,<sup>24,25</sup> the restoration of mitochondrial membrane potential and the inhibition of apoptosis by Tat-P hold significant implications for the prevention and treatment of BPD.

Previous studies, along with our experimental results, have consistently demonstrated that Tat-P can promote autophagy and inhibit apoptosis while repairing damaged alveolar epithelial cells. To further

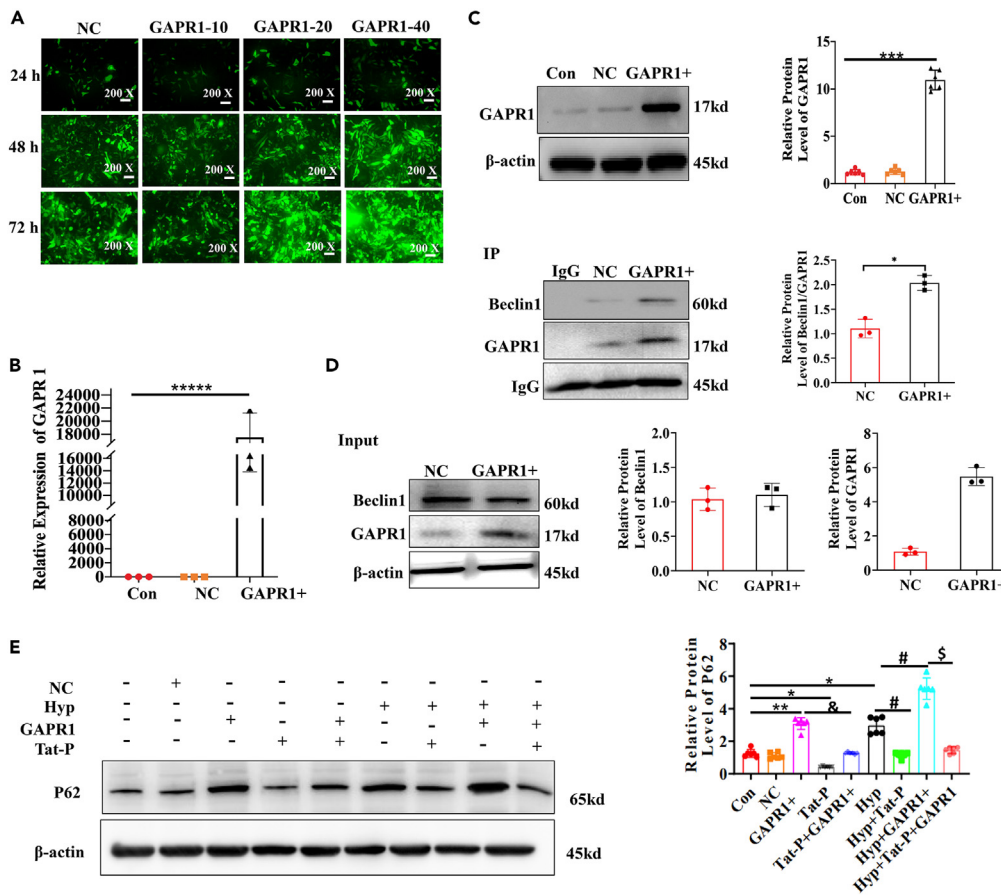


**Figure 7. Tat-p repairs the inhibition of cell autophagy induced by GAPR1 overexpression**

(A) Fluorescence microscopy was used to detect the overexpression efficiency of GAPR1 (1:10, 1:20, 1:40) at 24, 48, and 72h.

(B) RT-qPCR was used to detect the overexpression efficiency of GAPR1 (1:20) at 72h, N = 3.

(C) Western blot was used to detect the overexpression efficiency of GAPR1 (1:20) at 72h, N = 6.

(D) CO-IP was used to detect the combination effect of GAPR1 and Beclin1 in NC and GAPR1+ group.

(E) Western blot was used to detect the p62 protein expression in MLE-12 cells of Con, NC, GAPR1+, Tat-P, Tat-P + GAPR1+, Hyp, Hyp + GAPR1+, Hyp + Tat-P, Hyp + GAPR1+ and Hyp + Tat-P + GAPR1+ group, N = 6. Unpaired t-test, \*/#/\$/ <math>p < 0.05</math>, \*\*/##/\$\$/&& <math>p < 0.01</math>, \*\*\*/###/\$\$\$/&&& <math>p < 0.001</math>, \*\*\*\*/####/\$\$\$\$/&&&& <math>p < 0.0001</math>. NC: Negative control, Con: Control, Hyp: Hyperoxia, GAPR1+: GAPR1 overexpression. \* VS. Con or NC, # VS. Hyp, \$ VS. Hyp+GAPR1+, & VS. GAPR1+.

investigate the effects of Tat-P, we introduced two autophagy inhibitors, namely CQ and 3MA, to suppress autophagy. We found that Tat-P significantly counteracted the autophagy inhibiting effects of these inhibitors; however, its reparative effects on high oxygen exposure were attenuated. These findings provide further evidence that Tat-P exerts its beneficial effects in BPD by activating autophagy, inhibiting apoptosis, and repairing damaged alveolar epithelial cells.

Further investigation is needed to elucidate the underlying mechanism by which Tat-P promotes autophagy. Beclin1 plays a crucial role in the formation of autophagosomes.<sup>31</sup> Deletion of Beclin1 in lung epithelial cells during pregnancy's early or late stages in mice leads to fatal respiratory distress shortly after birth.<sup>5</sup> This condition is characterized by impaired airway branching, decreased formation of alveolar sacs, compromised vascularization, excessive epithelial cell death, reduced thinning of interstitial walls, delayed epithelial maturation, diminished peripheral alveolar sac formation and vascularization, and delayed distal epithelial differentiation. These pathological features bear resemblance to the manifestations observed in infants with BPD. Studies have shown that the interaction between Bcl-2 and Beclin1 plays a role in modulating autophagy to some extent.<sup>32</sup> Increased binding of Beclin1 to Bcl-2 inhibits autophagy, while decreased binding promotes

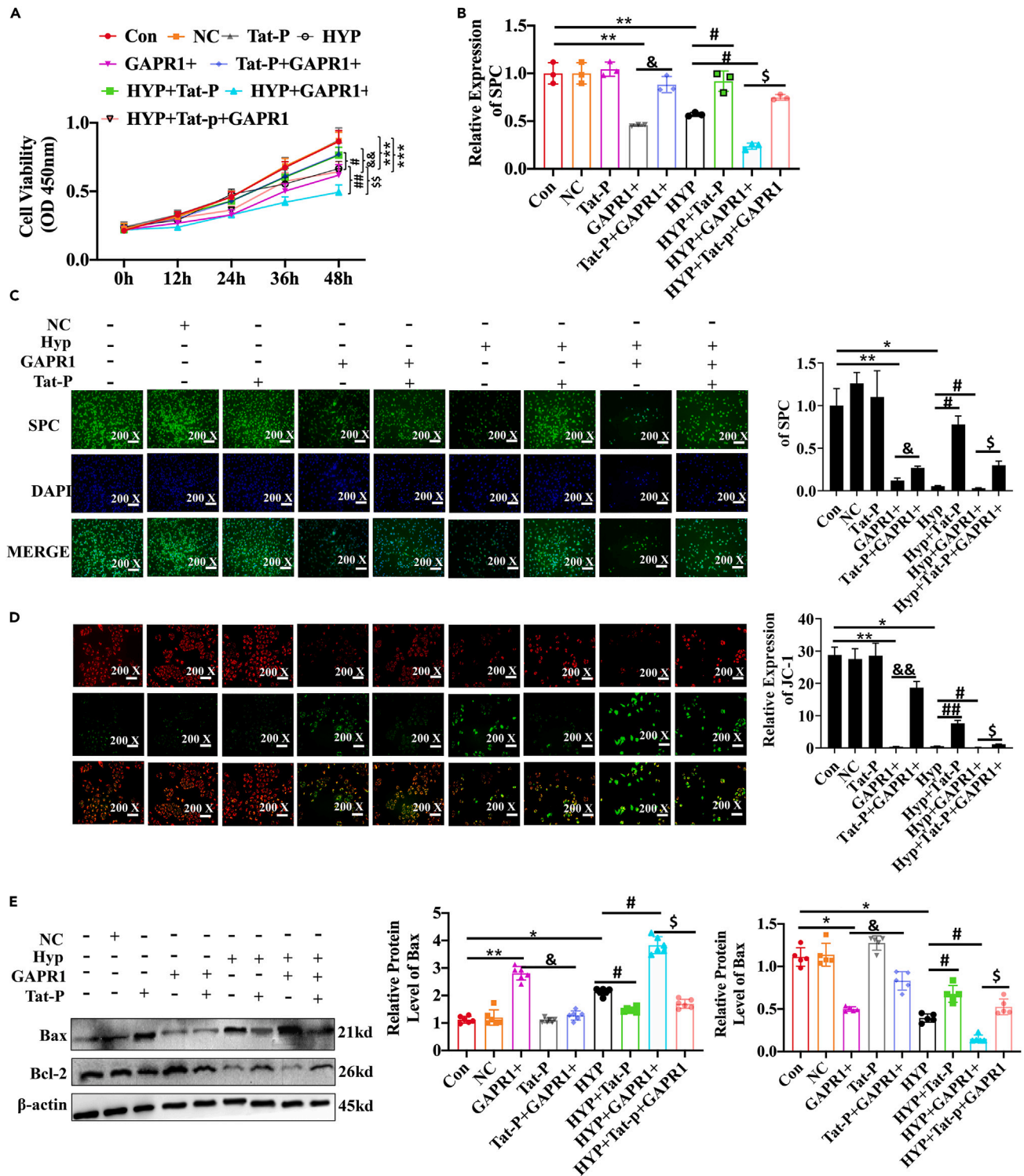


**Figure 8. Tat repairs alveolar epithelial cell damage caused by GAPR1 overexpression**

(A) CCK8 was used to detect cell viability in MLE-12 cells of Con, NC, Tat-P, GAPR1+, Hyp, Tat-P + GAPR1+, Hyp + Tat-P, Hyp + GAPR1+, Hyp + Tat-P and Hyp + Tat-P + GAPR1+ group, N = 3.

(B) RT-qPCR was used to detect the mRNA expression of SPC in MLE-12 cells of Con, NC, Tat-P, GAPR1+, Hyp, Tat-P + GAPR1+, Hyp + GAPR1+, Hyp + Tat-P and Hyp + Tat-P + GAPR1+ group, N = 6.

**Figure 8. Continued**

(C) Immunofluorescence was used to detect the SPC protein expression in MLE-12 cells of Con, NC, Tat-P, GAPR1+, Hyp, Tat-P + GAPR1+, Hyp + GAPR1+, Hyp + Tat-P and Hyp + Tat-P + GAPR1+ group, N = 6, bar = 200x.  
 (D) JC-1 kit was used to detect mitochondrial membrane potential in MLE-12 cells of Con, NC, Tat-P, GAPR1+, Hyp, Tat-P + GAPR1+, Hyp + GAPR1+, Hyp + Tat-P and Hyp + Tat-P + GAPR1+ group, N = 6. Red fluorescence indicates living cells that maintain mitochondrial membrane potential, while green fluorescence indicated cells that have undergone apoptosis or necrosis, bar = 200x.  
 (E) Western blot was used to detect the Bax and Bcl-2 protein level in MLE-12 cell line of Con, NC, Tat-P, GAPR1+, Hyp, Tat-P + GAPR1+, Hyp + GAPR1+, Hyp + Tat-P and Hyp + Tat-P + GAPR1+ group, N = 6. \*#/\$/& p < 0.05, \*\*##/\$/& p < 0.01, \*\*\*/###/\$\$/&& p < 0.001, \*\*\*\*/####/\$\$\$/&&& p < 0.0001. NC: Negative control, Con: Control, Hyp: Hyperoxia, GAPR1+: GAPR1 overexpression. \* VS. Con, # VS. Hyp, \$ VS. Hyp + GAPR1+, & VS. GAPR1+.

autophagy.<sup>33</sup> Consequently, compounds that disrupt the binding of Bcl-2 to Beclin1 or enhance the expression of Beclin1 can stimulate autophagy. As Tat-P is a small peptide molecule derived from the functional domain of the Beclin1 protein, we initially hypothesized that it may possess a structural domain similar to Beclin1 and could bind to Bcl-2, thereby reducing the binding between Beclin1 and Bcl-2 and promoting autophagy. However, our findings did not confirm the binding of Tat-P to Beclin1, and we did not observe any differences in Beclin1 protein expression among the different experimental groups.

To our knowledge, *Sanae Shoji-Kawata et al.* first indicated that Tat-P can competitively bind to the autophagy inhibitor GAPR1 protein, displacing Beclin1 protein, and activating autophagy.<sup>14</sup> The Class III phosphatidylinositol 3-kinase complex I (PtdIns3K-C1), comprising PIK3C3/VPS34, PIK3R4/VPS15, BECNL1, and ATG14 is a critical regulator of macrophage/autophagy induction.<sup>34</sup> GLIPR2 (also named GAPR1) has been identified as a negative regulator of PtdIns3K-C1 activity and basal autophagy by Yuting Zhao et al.<sup>35</sup> Our findings confirm that Tat-P binds to GAPR1 protein, leading to reduced binding between Beclin1 to GAPR1 protein. Moreover, a series of rescue experiments involving GAPR1 overexpression validate that Tat-P, in combination with GAPR1, releases Beclin1, thus promoting autophagy, inhibiting cell apoptosis, and repairing damaged alveolar epithelial cells. However, the specific mechanism underlying Tat-P-mediated autophagy promotion in BPD improvement requires further investigation. *Yanfei He et al.* demonstrated that the beneficial effects of Tat-P also rely on essential autophagy genes, as the absence of Atg5 abolishes the induced effect of Tat-P.<sup>36</sup> Based on these studies on Tat-P, it may further provide another ideas on the mechanism of Tat-P improving BPD.

We have preliminatively obtained the mechanism of Tat-P promoting autophagy, inhibiting apoptosis, repairing alveolar epithelial cell damage and improving the BPD cell model, and it is still necessary to further verify the effect of Tat-P on improving BPD *in vivo*. Alveolar epithelial cell damage is a pivotal factor contributing to the development of BPD.<sup>37-39</sup> Consequently, repairing the impaired alveolar epithelial cells represents a crucial therapeutic strategy for BPD. Previous studies have established that a BPD-like phenotype can be induced in neonatal mice subjected to 85% oxygen exposure for 7 days.<sup>40</sup> Building upon this model, we successfully established an animal model of BPD and our *in vivo* experiments corroborate the ability of Tat-P to ameliorate the phenotypic and surface marker alterations in alveolar epithelial cells in this BPD animal model.

**Conclusion**

In my opinion, this study is the first to investigate the role and mechanism of Tat-P in promoting autophagy through its binding to GAPR1 protein, thereby inhibiting apoptosis and repairing damaged alveolar

**Table 1. The primer sequences of circRNAs**

Primer name	Sequence
Rat SPC-F	GAGATGAGCATCGGAGGAGC
Rat SPC-R	AGGAGCCGCTGGTAGTCATA
Rat β-actin-F	CAGGGTGTGATGGTGGGTATGG
Rat β-actin-R	AGTTGGTGACAATGCCGTGTTC
Mouse SPC-F	ATGGAGAGTCCACCGGATTAC
Mouse SPC-R	ACCACGATGAGAAGGCGTTTG
Mouse β-actin-F	CCACAGCTGAGAGGGAATC
Mouse β-actin -R	TCTCCAGGGAGGAAGAGGAT

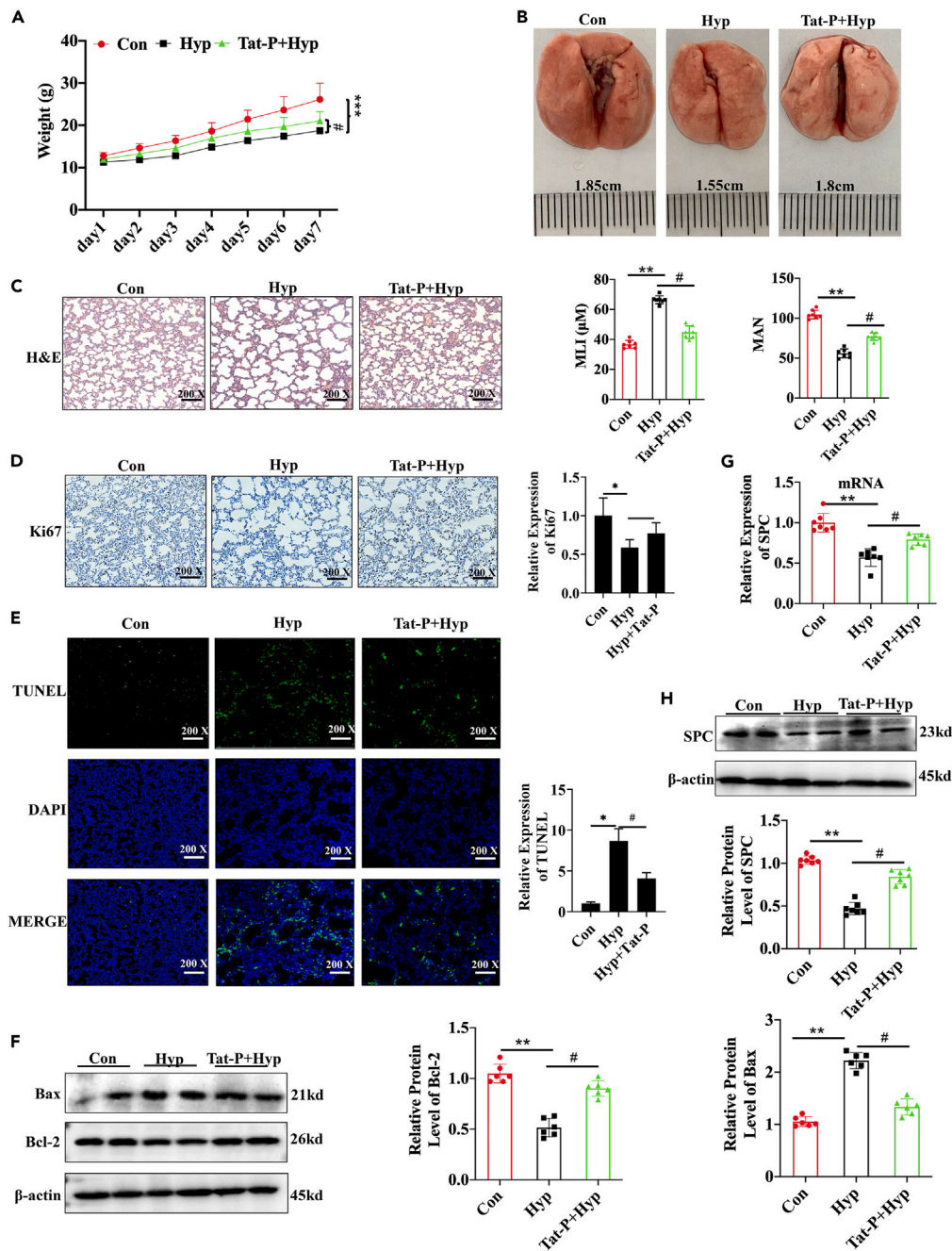


**Figure 9. Tat-P ameliorates the hyperoxia-induced BPD model in vivo**

A) The body weight change trend of pups at 1–7 days of Con, Hyp and Hyp+Tat-P groups N = 6.  
 B) Lung morphology of Con, Hyp and Hyp+Tat-P groups, N = 6.  
 C) Histopathological changes in the lung by H&E, N = 6, quantification of mean linear intercept (MLI) represents a surrogate of average air space diameter, quantification of mean alveolar number (MAN) represents the average number of alveoli.  
 D) Representative images of Ki67 immunostaining showing the proliferation (brown staining) in rat lung tissue of Con, Hyp and Hyp + Tat-P group, N = 6.  
 E) Representative images of TUNEL immunostaining showing the apoptosis (green staining) in rat lung tissue of Con, Hyp and Hyp + Tat-P group, N = 6.  
 F) Western blot used to detect the protein expression of Bax and Bcl-2 in rat lung tissue of Con, Hyp and Hyp + Tat-P group, N = 6.

**Figure 9. Continued**

(G) RT-qPCR detect the mRNA expression of SPC in Con, Hyp and Hyp + Tat-P group, N = 6.

(H). Western blot was used to detect the protein expression of SPC in Con, Hyp and Hyp + Tat-P group, N = 6. Unpaired t-test, \*/#/p < 0.05 , \*\*/##/p < 0.01, \*\*\*/###/p < 0.001, \*\*\*\*/####/p < 0.0001. Con: control, Hyp: Hyperoxia \* VS. Con, # VS. Hyp.

epithelial cells in the context of BPD. The findings of this study hold promise for the development of approaches for the prevention and treatment of BPD.

**Limitations of the study**

There also have been many limitations in our study, such as, we did not further explore the mechanism of Tat-P activation of autophagy and inhibition of apoptosis and, at the same time, we did not further optimize the Tat-P. Our team will further carry out relevant studies.

**STAR★METHODS**

Detailed methods are provided in the online version of this paper and include the following:

- KEY RESOURCES TABLE
- RESOURCE AVAILABILITY
  - Lead contact
  - Materials availability
  - Data and code availability
- EXPERIMENTAL MODEL AND STUDY PARTICIPANT DETAILS
  - Experimental animals
  - Ethical Statement
  - Animals models
  - Cell culture
- METHOD DETAILS
  - Peptide entry experiment (*in vitro* study)
  - Cell viability assay
  - Cell apoptosis
  - The reactive oxygen Species (ROS) assay
  - Mitochondrial membrane potential and apoptosis
  - Immunofluorescence
  - *In vivo* imaging
  - Western Blot
  - Peptide-protein pull-downing assay
  - Protein-protein pull-downing assay
  - Hematoxylin staining and immunohistochemistry
  - RNA isolation and RT-qPCR
- QUANTIFICATION AND STATISTICAL ANALYSIS

**SUPPLEMENTAL INFORMATION**

Supplemental information can be found online at <https://doi.org/10.1016/j.isci.2023.107509>.

**ACKNOWLEDGMENTS**

Top medical expert team of Wuxi Taihu Talent Program. (DJTD202106); Medical Key Discipline Program of Wuxi Health Commission (ZDXK2021007); Top Talent Support Program for young and middle-aged people of Wuxi Health Committee (BJ2020089); Project of Wuxi health Commission (Q202021); Wuxi Science and Technology Development Fund (N20202003, Y20212034). Project of Nantong Science and Technology Bureau (JC2021047). Nanjing Medical University Science and Technology development Fund (NMUB20210306). Medical Innovation Team of Wuxi Health Commission (CXTD2021005).

**AUTHOR CONTRIBUTIONS**

Z.Y., L.Z., and Z.Y. designed the research; Y.Z., Y.Z., and W.J. conducted the research and wrote the paper; R.Y. and F.Z. provided the samples; Y.F., T.T., J.C., S.C., and F.Z. analyzed data; All authors read and approved the final manuscript.

## DECLARATION OF INTERESTS

No conflict of interest.

## INCLUSION AND DIVERSITY

We support inclusive, diverse, and equitable conduct of research.

Received: December 8, 2022

Revised: June 25, 2023

Accepted: July 25, 2023

Published: August 2, 2023

## REFERENCES

- Hwang, J.S., and Rehan, V.K. (2018). Recent Advances in Bronchopulmonary Dysplasia: Pathophysiology, Prevention, and Treatment. *Lung* 196, 129–138. <https://doi.org/10.1007/s00408-018-0084-z>.
- Schmidt, A.R., and Ramamoorthy, C. (2022). Bronchopulmonary dysplasia. *Paediatr. Anaesth.* 32, 174–180. <https://doi.org/10.1111/pan.14365>.
- Principi, N., Di Pietro, G.M., and Esposito, S. (2018). Bronchopulmonary dysplasia: clinical aspects and preventive and therapeutic strategies. *J. Transl. Med.* 16, 36. <https://doi.org/10.1186/s12967-018-1417-7>.
- Warburton, D., and Bellusci, S. (2019). Normal lung development needs self-eating. *J. Clin. Invest.* 129, 2658–2659. <https://doi.org/10.1172/jci129442>.
- Yeganeh, B., Lee, J., Ermini, L., Lok, I., Ackerley, C., and Post, M. (2019). Autophagy is required for lung development and morphogenesis. *J. Clin. Invest.* 129, 2904–2919. <https://doi.org/10.1172/jci127307>.
- Zhang, D., Zhao, X., Zhang, D., Gao, S., Xue, X., and Fu, J. (2020). Hyperoxia reduces STX17 expression and inhibits the autophagic flux in alveolar type II epithelial cells in newborn rats. *Int. J. Mol. Med.* 46, 773–781. <https://doi.org/10.3892/ijmm.2020.4617>.
- Zhao, X., Shi, Y., Zhang, D., Tong, X., Sun, Y., Xue, X., and Fu, J. (2020). Autophagy inducer activates Nrf2-ARE pathway to attenuate aberrant alveolarization in neonatal rats with bronchopulmonary dysplasia. *Life Sci.* 252, 117662. <https://doi.org/10.1016/j.lfs.2020.117662>.
- Xu, H.D., and Qin, Z.H. (2019). Beclin 1, Bcl-2 and Autophagy. *Adv. Exp. Med. Biol.* 1206, 109–126. [https://doi.org/10.1007/978-981-15-0602-4\\_5](https://doi.org/10.1007/978-981-15-0602-4_5).
- Prerna, K., and Dubey, V.K. (2022). Beclin1-mediated interplay between autophagy and apoptosis: New understanding. *Int. J. Biol. Macromol.* 204, 258–273. <https://doi.org/10.1016/j.ijbiomac.2022.02.005>.
- Garcia, O., Hiatt, M.J., Lundin, A., Lee, J., Reddy, R., Navarro, S., Kikuchi, A., and Driscoll, B. (2016). Targeted Type 2 Alveolar Cell Depletion. A Dynamic Functional Model for Lung Injury Repair. *Am. J. Respir. Cell Mol. Biol.* 54, 319–330. <https://doi.org/10.1165/rncmb.2014-0246OC>.
- Chen, Y., Chang, L., Li, W., Rong, Z., Liu, W., Shan, R., and Pan, R. (2010). Thioredoxin protects fetal type II epithelial cells from hyperoxia-induced injury. *Pediatr. Pulmonol.* 45, 1192–1200. <https://doi.org/10.1002/ppul.21307>.
- Wu, D., Liang, M., Dang, H., Fang, F., Xu, F., and Liu, C. (2018). Hydrogen protects against hyperoxia-induced apoptosis in type II alveolar epithelial cells via activation of PI3K/Akt/Foxo3a signaling pathway. *Biochem. Biophys. Res. Commun.* 495, 1620–1627. <https://doi.org/10.1016/j.bbrc.2017.11.193>.
- Shoji-Kawata, S., Sumpter, R., Leveno, M., Campbell, G.R., Zou, Z., Kinch, L., Wilkins, A.D., Sun, Q., Pallauf, K., MacDuff, D., et al. (2013). Identification of a candidate therapeutic autophagy-inducing peptide. *Nature* 494, 201–206. <https://doi.org/10.1038/nature11866>.
- Li, Y., Zhao, Y., Su, M., Glover, K., Chakravarthy, S., Colbert, C.L., Levine, B., and Sinha, S.C. (2017). Structural insights into the interaction of the conserved mammalian proteins GAPR-1 and Beclin 1, a key autophagy protein. *Acta Crystallogr. D Struct. Biol.* 73, 775–792. <https://doi.org/10.1107/s2059798317011822>.
- Zhang, L., Soni, S., Hekimoglu, E., Berkelhamer, S., and Çataltepe, S. (2020). Impaired Autophagic Activity Contributes to the Pathogenesis of Bronchopulmonary Dysplasia. Evidence from Murine and Baboon Models. *Am. J. Respir. Cell Mol. Biol.* 63, 338–348. <https://doi.org/10.1165/rncmb.2019-0445OC>.
- Zhang, D., Wu, L., Du, Y., Zhu, Y., Pan, B., Xue, X., and Fu, J. (2018). Autophagy inducers restore impaired autophagy, reduce apoptosis, and attenuate blunted alveolarization in hyperoxia-exposed newborn rats. *Pediatr. Pulmonol.* 53, 1053–1066. <https://doi.org/10.1002/ppul.24047>.
- Cheong, H., Wu, J., Gonzales, L.K., Guttentag, S.H., Thompson, C.B., and Lindsten, T. (2014). Analysis of a lung defect in autophagy-deficient mouse strains. *Autophagy* 10, 45–56. <https://doi.org/10.4161/autophagy.26505>.
- Jin, R., Gao, Q., Yin, C., Zou, M., Lu, K., Liu, W., Zhu, Y., Zhang, M., and Cheng, R. (2022). The CD146-HIF-1 $\alpha$  axis regulates epithelial cell migration and alveolar maturation in a mouse model of bronchopulmonary dysplasia. *Lab. Invest.* 102, 794–804. <https://doi.org/10.1038/s41374-022-00773-z>.
- Hou, A., Fu, J., Shi, Y., Qiao, L., Li, J., Xing, Y., and Xue, X. (2018). Decreased ZONAB expression promotes excessive transdifferentiation of alveolar epithelial cells in hyperoxia-induced bronchopulmonary dysplasia. *Int. J. Mol. Med.* 41, 2339–2349. <https://doi.org/10.3892/ijmm.2018.3413>.
- Trembath, A., and Laughon, M.M. (2012). Predictors of bronchopulmonary dysplasia. *Clin. Perinatol.* 39, 585–601. <https://doi.org/10.1016/j.cip.2012.06.014>.
- Northway, W.H., Jr., Rosan, R.C., and Porter, D.Y. (1967). Pulmonary disease following respirator therapy of hyaline-membrane disease. Bronchopulmonary dysplasia. *N. Engl. J. Med.* 276, 357–368. <https://doi.org/10.1056/nejm196702162760701>.
- Wang, J., and Dong, W. (2018). Oxidative stress and bronchopulmonary dysplasia. *Gene* 678, 177–183. <https://doi.org/10.1016/j.gene.2018.08.031>.
- You, J., Zhou, O., Liu, J., Zou, W., Zhang, L., Tian, D., Dai, J., Luo, Z., Liu, E., Fu, Z., and Zou, L. (2020). Human Umbilical Cord Mesenchymal Stem Cell-Derived Small Extracellular Vesicles Alleviate Lung Injury in Rat Model of Bronchopulmonary Dysplasia by Affecting Cell Survival and Angiogenesis. *Stem Cells Dev.* 29, 1520–1532. <https://doi.org/10.1089/scd.2020.0156>.
- Cai, C., Qiu, J., Qiu, G., Chen, Y., Song, Z., Li, J., and Gong, X. (2017). Long non-coding RNA MALAT1 protects preterm infants with bronchopulmonary dysplasia by inhibiting cell apoptosis. *BMC Pulm. Med.* 17, 199. <https://doi.org/10.1186/s12890-017-0524-1>.
- Zhou, Y., Liu, Y., Xu, G., Liu, L., Li, H., Li, Y., Yin, J., Wang, X., and Yu, Z. (2022). Human breast milk-derived exosomes through inhibiting AT II cell apoptosis to prevent bronchopulmonary dysplasia in rat lung. *J. Cell Mol. Med.* 26, 4169–4182. <https://doi.org/10.1111/jcmm.17334>.
- Hallman, M., and Haataja, R. (2006). Surfactant protein polymorphisms and

- neonatal lung disease. *Semin. Perinatol.* **30**, 350–361. <https://doi.org/10.1053/j.semperi.2006.09.002>.
27. Zaib, S., Hayyat, A., Ali, N., Gul, A., Naveed, M., and Khan, I. (2022). Role of Mitochondrial Membrane Potential and Lactate Dehydrogenase A in Apoptosis. *Anti Cancer Agents Med. Chem.* **22**, 2048–2062. <https://doi.org/10.2174/1871520621666211126090906>.
  28. Estaquier, J., Vallette, F., Vayssiere, J.L., and Mignotte, B. (2012). The mitochondrial pathways of apoptosis. *Adv. Exp. Med. Biol.* **942**, 157–183. [https://doi.org/10.1007/978-94-007-2869-1\\_7](https://doi.org/10.1007/978-94-007-2869-1_7).
  29. Peña-Blanco, A., and García-Sáez, A.J. (2018). Bax, Bak and beyond - mitochondrial performance in apoptosis. *FEBS J.* **285**, 416–431. <https://doi.org/10.1111/febs.14186>.
  30. Edlich, F. (2018). BCL-2 proteins and apoptosis: Recent insights and unknowns. *Biochem. Biophys. Res. Commun.* **500**, 26–34. <https://doi.org/10.1016/j.bbrc.2017.06.190>.
  31. Tran, S., Fairlie, W.D., and Lee, E.F. (2021). BECLIN1: Protein Structure, Function and Regulation. *Cells*. <https://doi.org/10.103390/cells10061522>.
  32. Pattingre, S., Tassa, A., Qu, X., Garuti, R., Liang, X.H., Mizushima, N., Packer, M., Schneider, M.D., and Levine, B. (2005). Bcl-2 antiapoptotic proteins inhibit Beclin 1-dependent autophagy. *Cell* **122**, 927–939. <https://doi.org/10.1016/j.cell.2005.07.002>.
  33. Kang, R., Zeh, H.J., Lotze, M.T., and Tang, D. (2011). The Beclin 1 network regulates autophagy and apoptosis. *Cell Death Differ.* **18**, 571–580. <https://doi.org/10.1038/cdd.2010.191>.
  34. Chang, C., Young, L.N., Morris, K.L., von Bülow, S., Schöneberg, J., Yamamoto-Imoto, H., Oe, Y., Yamamoto, K., Nakamura, S., Stjepanovic, G., et al. (2019). Bidirectional Control of Autophagy by BECN1 BARA Domain Dynamics. *Mol. Cell* **73**, 339–353.e6. <https://doi.org/10.1016/j.molcel.2018.10.035>.
  35. Zhao, Y., Zou, Z., Sun, D., Li, Y., Sinha, S.C., Yu, L., Bennett, L., and Levine, B. (2021). GLIPR2 is a negative regulator of autophagy and the BECN1-ATG14-containing phosphatidylinositol 3-kinase complex. *Autophagy* **17**, 2891–2904. <https://doi.org/10.1080/15548627.2020.1847798>.
  36. He, Y., Lu, H., and Zhao, Y. (2022). Development of an autophagy activator from Class III PI3K complexes, Tat-BECN1 peptide: Mechanisms and applications. *Front. Cell Dev. Biol.* **10**, 851166. <https://doi.org/10.3389/fcell.2022.851166>.
  37. Bai, Y.X., Fang, F., Jiang, J.L., and Xu, F. (2017). Extrinsic Calcitonin Gene-Related Peptide Inhibits Hyperoxia-Induced Alveolar Epithelial Type II Cells Apoptosis, Oxidative Stress, and Reactive Oxygen Species (ROS) Production by Enhancing Notch 1 and Homocysteine-Induced Endoplasmic Reticulum Protein (HERP) Expression. *Med. Sci. Monit.* **23**, 5774–5782. <https://doi.org/10.12659/msm.904549>.
  38. Hou, A., Fu, J., Yang, H., Zhu, Y., Pan, Y., Xu, S., and Xue, X. (2015). Hyperoxia stimulates the transdifferentiation of type II alveolar epithelial cells in newborn rats. *Am. J. Physiol. Lung Cell Mol. Physiol.* **308**, L861–L872. <https://doi.org/10.1152/ajplung.00099.2014>.
  39. Ai, D., Shen, J., Sun, J., Zhu, Z., Gao, R., Du, Y., Yuan, L., Chen, C., and Zhou, J. (2022). Mesenchymal Stem Cell-Derived Extracellular Vesicles Suppress Hyperoxia-Induced Transdifferentiation of Rat Alveolar Type 2 Epithelial Cells. *Stem Cells Dev.* **31**, 53–66. <https://doi.org/10.1089/scd.2021.0256>.
  40. Pierro, M., Ionescu, L., Montemurro, T., Vadel, A., Weissmann, G., Oudit, G., Emery, D., Bodiga, S., Eaton, F., Péault, B., et al. (2013). Short-term, long-term and paracrine effect of human umbilical cord-derived stem cells in lung injury prevention and repair in experimental bronchopulmonary dysplasia. *Thorax* **68**, 475–484. <https://doi.org/10.1136/thoraxjnl-2012-202323>.

STAR★METHODS

KEY RESOURCES TABLE

REAGENT or RESOURCE	SOURCE	IDENTIFIER
<b>Antibodies</b>		
SPC	Proteintech	Cat# 10774-1-AP; RRID : AB_2185497
GAPR1	Santa	Cat# sc-398529; RRID : AB_2942027.
β-actin	Proteintech	Cat# 81115-1-RR; RRID : AB_2923704
LC3	Abcame	Cat# ab62721; RRID : AB_956136
P62	Proteintech	Cat# 13916-1-AP; RRID : AB_2267660
Bax	Proteintech	Cat# 50599-2-Ig; RRID : AB_2942026
BCL-2	Proteintech	Cat# 68103-1-Ig; RRID : AB_2942026
Beclin1	Proteintech	Cat# 11306-1-AP; RRID : AB_2259061
Ki67	CST	Cat# 34330; RRID : AB_2942026
HRP-conjugated Affinipure Goat Anti-Mouse IgG(H+L)	Proteintech	Cat# SA00001-1; SA00001-1
HRP-conjugated Affinipure Goat Anti-Rabbit IgG(H+L)	Proteintech	Cat# SA00001-2; RRID : AB_2722564
CoraLite488-conjugated Goat Anti-Mouse IgG(H+L)	Proteintech	Cat# SA00013-1; RRID : AB_2810983
<b>Bacterial and virus strains</b>		
GAPR1 overexpresses lentivirus	Gena pharma	N/A
<b>Chemicals, peptides, and recombinant proteins</b>		
Tat-P	Copeptide Biotechnology Co.	N/A
Tat-Scr	Copeptide Biotechnology Co.	N/A
GFP-Tat-P	Copeptide Biotechnology Co.	N/A
GFP- Scr	Copeptide Biotechnology Co.	N/A
Triton X-100	Beyotime	Cat# P0096
BSA	Beyotime	Cat# ST025
TUNEL	Beyotime	Cat# C1086
DAPI	Beyotime	Cat# C1002
RIPA	Beyotime	Cat# P0013B
Protease inhibitor cocktail and phosphatase inhibitor	Beyotime	Cat# P1046
Primary antibody diluent	Servicebio	Cat# G2025
CQ	sigma	Cat# C6628
3MA	sigma	Cat# M9281
Streptavidin magnetic beads	Life	Cat# 11205D
Protein A/G beads	Life	Cat# 88803
IP buffer	Beyotime	Cat# P0013
DMEM/F12	Gibco	Cat# 11320033
FBS	Gibco	Cat# 10099141C
penicillin-streptomycin	Gibco	Cat# 15070063
<b>Critical commercial assays</b>		
Cell counting kit-8 (CCK-8)	Dojindo	Cat# CK04
Annexin V/PI Apoptosis Detection Kit I	BD Biosciences Pharmingen	Cat# 556547
Reactive Oxygen Species Assay Kit	Beyotime	Cat# S0033S
Mitochondrial Membrane Potential and Apoptosis Detection Kit	Beyotime	Cat# C2006

(Continued on next page)

<b>Continued</b>		
<b>REAGENT or RESOURCE</b>	<b>SOURCE</b>	<b>IDENTIFIER</b>
bicinchoninic acid (BCA) assay kit	Beyotime	Cat# P0012
Vectastain kit	Vectorlabs	Cat# PK-6100
RNAeasy kit	Tiangen	Cat# DP451
iScript cDNA Synthesis Kit	Takara	Cat# RR047A
<b>Experimental models: Cell lines</b>		
MLE-12	ATCC	BH-C465
<b>Experimental models: Organisms/strains</b>		
Lung/Liver/ spleen of SD pups	Animal Center of Nanjing Medical University	N/A
<b>Oligonucleotides</b>		
Primers for the study, see <a href="#">Table 1</a>	This paper	N/A
<b>Software and algorithms</b>		
ImageJ	Schneider et al.	<a href="https://imagej.nih.gov/ij/">https://imagej.nih.gov/ij/</a>
Graph Pad Prism 9	Graphpad Software	<a href="https://www.graphpad.com">https://www.graphpad.com</a>
FlowJo Version	BD Biosciences Pharmingen	<a href="https://www.bdbiosciences.com">https://www.bdbiosciences.com</a>
<b>Other</b>		
Hyperoxic chamber of cell	This paper	N/A
Hyperoxic chamber of animal	This paper	N/A

## RESOURCE AVAILABILITY

### Lead contact

Lead Contact Requests for related resources or information will be addressed by the lead contact, Dr. Yahui Zhou ([yahuizhou@njmu.edu.cn](mailto:yahuizhou@njmu.edu.cn)).

### Materials availability

This study did not generate new unique reagents.

### Data and code availability

- All data reported in this paper will be shared by the [lead contact](#) upon request.
- This paper does not report original code.
- Any additional information required to reanalyze the data reported in this paper is available from the [lead contact](#) upon request.

## EXPERIMENTAL MODEL AND STUDY PARTICIPANT DETAILS

### Experimental animals

Experiments were performed in SD pups, male and female rats, aged 1 to 7 days old. Male and female mice were analyzed. Gender as a social construct was not applicable to our study.

### Ethical Statement

The SD rats employed in this investigation were procured from the Animal Center of Nanjing Medical University. The study protocol was approved by the Animal Research and Care Committee of Nanjing Medical University, with the permission number IACUC-1907021.

### Animals models

Neonatal SD rats and their mothers were housed in a sealed plexiglass chamber (China) from postnatal day 1 to day 7. The animal model of BPD was established by continuously supplying 85% oxygen into the chamber. The control group received normal oxygen in the same room. To mitigate the influence of maternal rats on the offspring, the mothers in the control and model groups were swapped daily. In the experimental

group, 85 % oxygen-exposed pups were intraperitoneally injected with 200  $\mu\text{g}/\text{kg}$  of Tat-P or Tat-S at 9:00 and 16:00 each day.

### Cell culture

*In vitro* experiments were conducted using murine lung epithelial cells (MLE-12, ATCC). These cells were cultured in Dulbecco's Modified Eagle Medium: Nutrient Mixture F12 (DMEM: F-12) supplemented with 10% fetal bovine serum (Gibco, USA) and 1% penicillin-streptomycin (Gibco, USA). The cells were maintained at 37°C with 5%CO<sub>2</sub>. For the experimental groups, the normal oxygen group was exposed to 21% oxygen, while the hyperoxia group was exposed to 85% oxygen. Peptide interventions were performed at concentrations of 1  $\mu\text{M}$ , 2.5  $\mu\text{M}$ , and 5  $\mu\text{M}$ . The optimal concentration was determined based on cell viability and apoptosis results, which was found to be 5  $\mu\text{M}$ . The concentration of CQ (chloroquine) used was 50  $\mu\text{M}$ , while 3MA (3-methyladenine) was used at a concentration of 5 mM. Lentiviral gradients of GAPR1 were prepared at ratios of 1:10, 1:20, and 1:40.

## METHOD DETAILS

### Peptide entry experiment (*in vitro* study)

Tat-P and Tat-Scr were fluorescently labeled using a green fluorescent protein (GFP) from Copeptide Biotechnology Co., LTD. MLE-12 cells were seeded on 6-well plates and allowed to attach for 24 h. Subsequently, the cells were treated with a solution containing GFP, GFP-labeled Tat-P and GFP-labeled Tat-Scr for 3 h. The entry of the peptides into the cells was visualized using a fluorescence microscope (Zeiss, Germany).

### Cell viability assay

Cell viability was assessed using the cell counting kit-8 (CCK-8) (Dojindo, Japan) according to the manufacturer's instructions. MLE-12 cells were seeded uniformly in 96-well plates at a concentration of  $1 \times 10^3$  cells per well. After cell adhesion, the cells were treated with Tat-P, Scr-Tat-P, CQ, and GAPR1 for 0, 12, 24, 36, and 48 h. The optical density (OD) was measured at 450 nm using a microplate reader (BioTek Instruments Inc., Germany).

### Cell apoptosis

The Annexin V/PI Apoptosis Detection Kit I (BD Biosciences Pharmingen, USA) was utilized to assess cell apoptosis. Initially, approximately 30,000 cells were seeded in six-well plates, washed with 2 mL of cold phosphate-buffered saline (PBS), and harvested by centrifugation. The cells were then resuspended in 100  $\mu\text{L}$  of 1X binding buffer on ice. Subsequently, Annexin V (5  $\mu\text{L}$ ) and propidium iodide (5  $\mu\text{L}$ , 1 mg/mL) were added in the dark and incubated on ice for 15 min (or less than 1 h). Finally, cell apoptosis was analyzed using a flow cytometer (Becton Dickinson, USA) and FlowJo Version 8.6 software.

### The reactive oxygen Species (ROS) assay

The oxidative stress index was evaluated using a Reactive Oxygen Species Assay Kit (ROS Assay Kit, Beyotime, china). DCFH-DA was diluted with a serum-free medium at a ratio of 1:1000 to achieve a final concentration of 10  $\mu\text{M}$ . The cells were harvested and resuspended in the diluted DCFH-DA solution at a concentration of  $1 \times 10^6$  cells/mL. Following that, the cell suspension was incubated at 37°C in a cell culture incubator for 20 min. To ensure full contact between the probe and the cells, the cell suspension was gently mixed by inverting it every 3-5 min. Subsequently, the cells were washed three times with a serum-free cell culture medium to completely remove any residual DCFH-DA that had not entered the cells. Finally, the cells were directly stimulated with either a reactive oxygen positive control or Tat-P, and the analysis was performed using a flow cytometer (Becton Dickinson, USA) and FlowJo Version 8.6 software.

### Mitochondrial membrane potential and apoptosis

The Mitochondrial Membrane Potential and Apoptosis Detection Kit (Beyotime, China) is a dual-staining kit that utilizes a red fluorescence probe (Mito-Tracker Red CMXRos) dependent on mitochondrial membrane potential and a green fluorescence probe (Annexin V-FITC) to detect apoptosis and mitochondrial membrane potential in cultured cells. Red fluorescence indicates viable cells with intact mitochondrial membrane potential, while green fluorescence indicates cells undergoing apoptosis or necrosis. To perform the staining, cells were initially cultured in 24-well plates. The culture medium was removed, and the cells were washed with PBS. Subsequently, 188  $\mu\text{L}$  of Annexin V-FITC binding solution and 5  $\mu\text{L}$  of Annexin

V-FITC were added and gently mixed. Then, 2  $\mu$ L of Mito-Tracker Red CMXRos staining solution was added and mixed gently. The cells were incubated in the dark at room temperature (20°C - 25°C) for 30 min, while precautions were taken to protect against light exposure, such as using aluminum foil. Finally, the stained cells were observed under a fluorescence microscope (Zeiss, Germany). It is recommended to visualize the stained cells promptly, typically within 1 h after staining.

### Immunofluorescence

The cells in the six-well plate were initially fixed with 4% paraformaldehyde for 30 min. Subsequently, they were washed three times with PBS for 5 min each. The cells underwent permeabilization and blocking using 0.2% Triton X-100/PBS and 5% bovine serum albumin (BSA)/PBS, respectively. For immunostaining, the cells were treated with SPC antibody (Proteintech), at a dilution of 1:200 in 1% BSA, and incubated overnight at 4°C. The following day, the cells were washed three times with PBS at 4°C for 5 min each. They were then incubated with secondary antibodies (goat anti-rabbit) labeled with fluorescence, at a dilution of 1:1000 for 2 h. After another three washes with PBS, for 5 min each, the cells were stained with DAPI (1:1000) for 5 min. Subsequently, the cells were washed three times with PBS for 5 min each, and images were captured using a fluorescence microscope (Zeiss, Germany).

### In vivo imaging

GFP-labeled Tat-P was administered to the pups via intraperitoneal injection, while pups injected with normal saline served as the control group. The whole-body fluorescence intensity of the pups was assessed using an *In vivo* imaging system (IVIS Spectrum, PerkinElmer, USA), and various organs were collected for imaging purposes.

### Western Blot

For western blot analysis, the sample size was either  $n = 3$  or  $n = 6$ . Cells or lung tissue homogenate samples were lysed on ice using a radioimmunoprecipitation assay (RIPA) buffer containing a protease inhibitor cocktail and phosphatase inhibitor for 30 min. The supernatant was collected after centrifugation at 12,000 rpm and 4°C for 30 min. Protein concentration was determined using a bicinchoninic acid (BCA) assay kit. Subsequently, 30  $\mu$ g of protein lysate was subjected to gel electrophoresis. The proteins were then transferred to a polyvinylidene fluoride membrane, which was blocked with 5% skim milk and incubated at room temperature for 2 h with shaking. The membrane was incubated overnight at 4°C with primary antibodies diluted in primary antibody diluent according to the manufacturer's instructions. The following primary antibodies and dilutions were used: SPC (Proteintech, 1:1000),  $\beta$ -actin (Proteintech, 1:1000), Bax (Proteintech, 1:1000), Bcl-2 (Proteintech, 1:1000), GAPR1 (Santa, 1:100), Beclin1 (Proteintech, 1:1000), P62 (Proteintech, 1:1000), and LC3 (Abcam, 1:1000). The next day, the membrane was washed three times for 10 min each with TBS-T. Subsequently, the membrane was incubated with a secondary antibody (goat anti-rabbit or goat anti-mouse isotype: IgG HRP-conjugate, Proteintech 1:5000) under shaking conditions for 1 h at room temperature. After three washes with TBS-T for 10 min each, an enhanced chemiluminescence detection kit was used for signal development, and the images were captured using a ChemiDoc™ XRS + Imager (Bio-RAD, Hercules, CA, USA).

### Peptide-protein pull-down assay

To perform peptide-protein pull-down assays, streptavidin magnetic beads (Life, USA) were chilled on ice, and 30  $\mu$ L was added to the corresponding EP tubes containing Tat-P and Scr-Tat-P. The EP tubes were placed on a magnetic rack until the solution became clear, and the supernatant was discarded. Then, 1 ml of RIPA and PMSF (100:1) solution was added to the beads, and the mixture was placed on the magnetic rack. This process was repeated three times, and the supernatant was discarded. Subsequently, an appropriate amount of RIPA buffer and peptides (200  $\mu$ g) was added and the solution was placed in a refrigerator at 4°C with shaking. The following day, the magnetic beads bound to the peptides were separated using the magnetic rack. Once the solution turned clear, the supernatant was discarded, and new RIPA lysate was added. After mixing, the solution was removed, and the supernatant was discarded. This process was repeated for the final supernatant removal. Protein lysate (2 mg/EP tube) was then added, and after mixing, the mixture was incubated overnight at 4°C with shaking. On the subsequent day, the magnetic beads, peptides, and proteins were taken out and placed on the magnetic rack until the solution became clear. The supernatant was discarded, and new RIPA buffer was added, followed by placing the solution on the magnetic rack. This step was repeated 6 times. Finally, 30  $\mu$ L of 1x SDS was added, and the solution was heated

at 95°C for 5 min. The prepared magnetic beads, peptides and protein complexes were stored at -80°C until further use.

### Protein-protein pull-down assay

For the Protein-Protein Pull-down assay, protein A/G beads (Life, USA) were preincubated with the GAPR1 antibody or IgG. Subsequently, lysed with IP buffer (Beyotime, China). After centrifugation, the supernatant was incubated with the beads at 4°C overnight. Finally, the beads were washed, SDS buffer was added, and the immunoprecipitates were determined by western blot analysis.

### Hematoxylin staining and immunohistochemistry

On the 7<sup>th</sup> day of the experimental period, the rats were euthanized, and their lung tissues were collected. The right lung was fixed in 4% paraformaldehyde solution (pH 7.4, 20 cm H<sub>2</sub>O) for a minimum of 2 h. The lung was divided into 3 parts, and 3 μm sections were cut from top to bottom for hematoxylin and eosin (H&E) staining. For immunohistochemistry (IHC), 4 μm sections of lung tissue were prepared and dewaxed. Antigen retrieval was performed by treating the sections with a 10 mM citric acid buffer (pH 6.0) and subjecting them to pressure cooking for 10 min. Endogenous peroxidase activity was quenched by incubating the sections with a 0.5% H<sub>2</sub>O<sub>2</sub>/methanol solution for 15 min, followed by blocking with 1.5% rabbit serum in PBS (Science Cell, China) for 30 min. The slides were then incubated with primary antibodies, including goat anti-mouse Ki67 (CST, 1:100 dilution) and TUNEL and incubated, at room temperature (23°C - 25°C) for 1 h. Subsequently, the slides were incubated with a secondary antibody and stained with diaminobenzidine according to the instructions provided with the Vectastain kit. Finally, the slides were scanned using an Aperio scanner (ePathology solution).

### RNA isolation and RT-qPCR

Total RNA was extracted using TRIzol (Life, USA) and the RNAeasy kit (Tiangen, China). The iScript cDNA Synthesis Kit (Takara, Japan) was used to synthesize the first strand of cDNA according to the RT-qPCR instructions. The cDNA samples were then subjected to PCR amplification with SYBR Green (Life, USA) in a reaction volume of 20 μL. The primers used are provided in Table 1. The amplification was carried out in a real-time system (Applied Biosystems, USA) with an initial step of 10 min at 95°C, followed by denaturation at 94°C for 15 s, annealing at 54°C for 30 s, and extension at 72°C for 40 s.

### QUANTIFICATION AND STATISTICAL ANALYSIS

The data are presented as mean ± standard deviation (SD). Statistical analysis was performed using a two-tailed Student's t-test to determine the significance between two groups, while a one-way analysis of variance (ANOVA) was conducted for multiple comparisons, depending on the number of variables (GraphPad Prism9). A *P*-value of < 0.05 was considered statistically significant, \*/#/\$/& P < 0.05, \*\*/##/\$\$/&& P < 0.01, \*\*\*/###/\$\$\$/&&& P < 0.001, \*\*\*\*/####/\$\$\$\$/&&&& P < 0.0001.